Available online at www.sciencedirect.com
SCIENCE DIRECT®
Catalysis Today 105 (2005) 401–406
CATALYSIS TODAY
www.elsevier.com/locate/cattod

# Conceptual design and CFD simulation of a novel metal-based monolith reactor with enhanced mass transfer

Hui Liu *, Jundong Zhao, Chengyue Li, Shengfu Ji

*The Key Lab of Science and Technology of Controllable Chemical Reactions, Ministry of Education, Beijing University of Chemical Technology, Beijing 100029, China*

**Abstract**

This paper introduces a novel structured metallic catalyst that improves mass transfer performance of a monolith reactor for highly exothermic gas–solid reactions. The monolith channels are designed to have metallic substrates that consist of two layers with one of the layers being the metallic support and another layer being a foam metal annular that is tightly deposited onto the support surface by some means. Parametrical studies based on a 2D monolith reactor model showed that the present design yields an enhanced mass transfer between the bulk fluid and the catalyst layer due to a decrease in external film resistance, and an enhanced mass transfer within the solid phase mainly due to the viscous flow effect within the porous catalyst layer.


*Keywords:* Monolith catalysts; Structured catalysts; Reactor modeling; Catalyst design; Catalytic combustion; Mass transfer

## 1. Introduction

Monolith reactors are becoming increasingly significant as catalyzed gas–solid or multiphase reactors in view of the advantages they offer in comparison to conventionally used packed beds, and trickle beds for a host of processes. These advantages, generally speaking, include low-pressure drop, high heat and mass transfer rates and minimum axial dispersion stem from the uniquely structured multi-channel configuration of monoliths. A number of studies have focused on the use of honeycomb monolith reactors for environmental catalysis, for example, catalytic combustion reactions, and gas–solid processes for chemicals production [1–4].

In essence, a monolith block is composed of an array of uniformly structured parallel channels often of square or circular geometry, typically having hydraulic diameters between 1 and 5 mm. The substrate material may be either ceramic or metallic. In honeycomb monolith reactors, the catalyst is often dispersed within a washcoat that is coated onto the surface, or may be contained within the substrate material. Some studies have shown that the utilization of metallic substrates can greatly enhance heat transfer for highly exothermal catalytic gas solid reactions carried out in a monolith reactor. It is well known that catalytic gas solid reactions in such channels may be controlled by the external mass transfer step near the (bulk) gas solid interfaces and/or the diffusion step within the washcoat or substrate, depending on transport and reaction conditions encountered [5]. Modeling efforts and experimental investigations directed to these aspects were frequently reported to show the effects of the mass transfer steps on the reactor performances of catalytic combustion reactions and the oxidation of light hydrocarbons, mainly in viewing the loading of active element(s), the shape of the substrate and the operating conditions, etc. [5–12].

The objective of the present work is to present a novel conceptual design of monolith reactors with enhanced mass transfer characteristics. This can be accomplished by inserting high-thermal conductivity porous substrates on the inner tube wall of the monolith support. A reactor model is constructed to simulate the system under consideration to study the mass transfer and reaction performances of the monolith reactor.

* Corresponding author. Tel.: +86 10 64433695.
*E-mail address:* hliu@mail.buct.edu.cn (H. Liu).

0920-5861/$ – see front matter © 2005 Elsevier B.V. All rights reserved.
doi:10.1016/j.cattod.2005.06.060

**Nomenclature**

| | |
|---|---|
| $a$ | parameters defined in Eq. (1) |
| $C_A$ | concentration (mol/m$^3$) |
| $C_p$ | thermal capacity (J/kg K) |
| $D$ | mass diffusivity (m$^2$/s) |
| $F$ | Forchheimer coefficient |
| $k$ | thermal conductivity (W/(m K)) |
| $k_V$ | rate constant (1/s) |
| $K$ | permeability (m$^2$) |
| $L$ | channel length (m) |
| $L_C$ | characteristic length of catalyst (m) |
| $P$ | pressure (Pa) |
| $r$ | radial coordinate (m) |
| $r_{AS}$ | surface reaction rate (mol/s m$^2$) |
| $r_{AC}$ | reaction rate (mol/s m$^3$) |
| $Y_A$ | volume fraction (%) |
| $R$ | radius (m) |
| $S$ | source terms defined in Eq. (1) |
| $Sh$ | Sherwood number |
| $T$ | temperatures (K) |
| $u$ | axial velocity component (m/s) |
| $v$ | radial velocity component (m/s) |
| $x$ | axial coordinate (m) |

*Greek symbols*

| | |
|---|---|
| $\varepsilon$ | porosity of porous layer |
| $\phi$ | generic transport property defined in Eq. (1) |
| $\phi_L$ | generalized Thiele modulus |
| $\eta$ | effective factor |
| $\mu$ | viscosity (Pa s) |
| $\rho$ | density (kg/m$^3$) |
| $\tau$ | tortuosity of catalyst |
| $\Gamma$ | transport coefficient defined in Eq. (1) |

*Subscripts*

| | |
|---|---|
| 0 | inlet |
| b | bulk phase |
| $i$ | variable ($i = 1$, axial velocity; $i = 2$, radial velocity; $i = 3$, temperature; $i = 4$, concentration) |
| i | interface |
| $j$ | phase ($j = 1$, bulk phase; $j = 2$, porous layer) |

## 2. Model development

### 2.1. Physical model and assumptions

We consider a circular monolith channel designed to have metallic substrates that consist of two layers, as shown in Fig. 1. One of the layers is the metallic support which constitutes the matrices as in a conventional honeycomb monolith. Another layer is a foam metal annular that is tightly deposited onto the support surface by some means. This layer is a similar counterpart of the conventionally used washcoat, wherein the catalyst may be coated. The rational behind the design is that: (1) the high thermal diffusivity of the metallic base substrate provides an effective radial heat transfer between channels; and (2) the foam metal layer containing catalytically active element(s) can effectively enhance the mass transfer both for the external mass transfer and the diffusion within layer as discussed later.

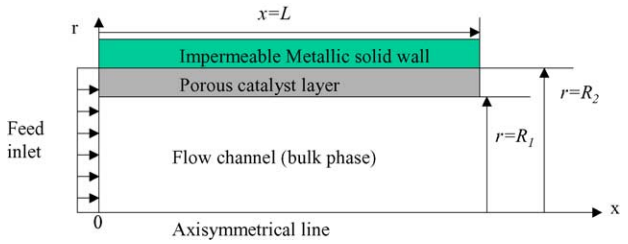


Fig. 1. Single channel configuration.

Catalytic combustion of methane was selected as the model reaction. A first-order rate expression was used for the reaction within the porous layer and on the impermeable solid wall. Because the monolith can be viewed as a structure made up of a number of repeating building blocks where the basic building block is a single channel, it can be argued that the reactor model on a single channel can be employed in scaling up a monolith reactor provided that a uniform gas distribution and adiabatic circumstance of the monolith as a whole are assumed. Additional assumptions include: (1) the channel is cylindrical and the flow is axisymmetric and laminar, (2) the porous medium is homogeneous, isotropic, and saturated with a single phase fluid, (3) the interactions between the porous medium and the clear fluid is simulated by the Darcy–Brinkman–Forchheimer formulation [13], (4) the solid matrix and the fluid are assumed to be at local thermal and concentration equilibrium with each other, and (5) homogeneous reaction and heat radiation in the bulk phase are ignored.

### 2.2. Governing equations

Two sets of axisymmetric 2D governing equations were set up for the bulk gas phase and the porous solid phase including momentum, heat and mass balance equations. Particularly, the porous substrate phase is described by the Darcy–Brinkman–Forchheimer model to take into account of the viscous flow effect in addition to diffusion within the catalyst layer [13]. For axisymmetric steady state flow in a circular tube the radial and axial components governing equations in their conservative form were

$$\frac{\partial(a_{i,j}u_j\phi_{i,j})}{\partial x}+\frac{1}{r}\frac{\partial(ra_{i,j}v_j\phi_{i,j})}{\partial r} = \frac{\partial}{\partial x}\left(\Gamma_{i,j}\frac{\partial\phi_{i,j}}{\partial x}\right)+\frac{1}{r}\frac{\partial}{\partial r}\left(r\Gamma_{i,j}\frac{\partial\phi_{i,j}}{\partial r}\right)+S_{i,j} \quad (1)$$

Table 1
Parameters and source terms for the conservation equations given by Eq. (1)

| Domains | Equations | $\phi_{i,j}$ | $a_{i,j}$ | $\Gamma_{i,j}$ | $S_{i,j}$ |
|---|---|---|---|---|---|
| Bulk phase ($j = 1$) | Continuity | 1 | $\rho_1$ | 0 | 0 |
| | Axial-momentum | $u_1$ | $\rho_1$ | $\mu_1$ | $-\frac{\partial P}{\partial x}$ |
| | Radial-momentum | $v_1$ | $\rho_1$ | $\mu_1$ | $-\frac{\partial P}{\partial r} - \frac{2\mu_1 v_1}{r^2}$ |
| | Energy balance | $T_1$ | $\rho_1\, C_{P1}$ | $k_1$ | 0 |
| | Mass balance | $C_{A1}$ | 1 | $D_{AB,1}$ | 0 |
| Porous phase ($j = 2$) | Continuity | 1 | $\rho_2$ | 0 | 0 |
| | Axial momentum | $u_2$ | $\rho_2$ | $\mu_2$ | $-\frac{\partial P}{\partial x} - \frac{\mu_2}{K} u_2 - \frac{F_\varepsilon}{\sqrt{K}} \rho_2 u_2^2$ |
| | Radial momentum | $v_2$ | $\rho_2$ | $\mu_2$ | $-\frac{\partial P}{\partial r} - \frac{2\mu_2 v_2}{r^2} - \frac{\mu_2}{K} v_2 - \frac{F_\varepsilon}{\sqrt{K}} \rho_2 v_2^2$ |
| | Energy balance | $T_2$ | $\rho_2\, C_{P2}$ | $k_2$ | $+(-r_{AC})(-\Delta H)$ |
| | Mass balance | $C_{A2}$ | 1 | $D_{AB,2}$ | $-(-r_{AC})$ |

where $\phi_{i,j}$ represents generic transport properties (see Table 1), i.e., $u_j$ and $v_j$ are velocity components ($i$ = 1,2), $T_j$ are temperatures ($i = 3$), and $C_{Aj}$ are concentrations ($i = 4$) in the bulk phase ($j = 1$) and the catalyst layer ($j = 2$), respectively; and $a_{i,j}$ are parameters, $S_{i,j}$ are source terms and $\Gamma_{i,j}$ are the transport coefficient of the variables in the phase $j$. Besides, $K$ is permeability and $\varepsilon$ the porosity of the porous layer, and $F$ is the Forchheimer coefficient which is given by [14]

$$F = \frac{1.8}{\sqrt{180\varepsilon^5}} \tag{2}$$

### 2.3. Boundary conditions and numerical method

The boundary conditions used were as the following:

(1) At the inlet of the channel

$$u_1 = u_2 = U_0;\ \ v_1 = v_2 = 0;\ \ C_{A1} = C_{A2} = C_{A0};\ \text{and}\ \ T_1 = T_2 = T_0 \tag{3}$$

(2) At the axisymmetric line of the channel

$$\frac{\partial u_1}{\partial r} = \frac{\partial v_1}{\partial r} = 0;\ \ \frac{\partial C_{A1}}{\partial r} = 0;\ \ \text{and}\ \ \frac{\partial T_1}{\partial r} = 0 \tag{4}$$

(3) At the outlet of the channel

$$\frac{\partial u_1}{\partial r} = \frac{\partial v_1}{\partial r} = 0;\ \ \frac{\partial C_{A1}}{\partial z} = \frac{\partial C_{A2}}{\partial z} = 0;\ \ \text{and}\ \ \frac{\partial T_1}{\partial z} = \frac{\partial T_2}{\partial z} = 0 \tag{5}$$

(4) At the impermeable wall

$$u_2 = 0;\ \ v_2 = 0 \tag{6}$$

$$-D_{AB,2}\frac{\partial C_{A2}}{\partial r} = (-r_{AS});\ \ \text{and}\ \ k_2\frac{\partial T_2}{\partial r} = (-r_{AS})(-\Delta H) \tag{7}$$

where $r_{AS}$ is the surface reaction rate.

### 2.4. Additional relations

The rate expression used for the surface reaction was [8]

$$-r_{AS} = 3 \times 10^5 \exp\left(-\frac{90,000}{RT}\right) C_{A2} \qquad (\text{mol/m}^2\,\text{s}) \tag{8}$$

and

$$-r_{AC} = 3 \times 10^8 \exp\left(-\frac{90,000}{RT}\right) C_{A2} \qquad (\text{mol/m}^3\,\text{s}) \tag{9}$$

for the porous layer reaction [12].

The diffusion coefficient for methane in air was calculated from the Fuller correlation [8]:

$$D_{AB,j} = 9.99 \times 10^{-5}\frac{T_j^{1.75}}{P} \qquad (\text{m}^2/\text{s}) \tag{10}$$

and

$$D_{AB,2} = \frac{\varepsilon}{\tau} D_{AB,1} \tag{11}$$

The viscosity of the fluid was computed from [8]

$$\mu_j = 7.701 \times 10^{-6} + 4.166 \times 10^{-8} T_j - 7.531 \times 10^{-12} T_j^2 \quad (\text{Pa}\,\text{s}) \tag{12}$$

and

$$\mu_1 = \mu_2 \tag{13}$$

The thermal conductivity of the fluid was calculated by [8]

$$k_j = 1.679 \times 10^{-2} + 5.073 \times 10^{-5} T_j \qquad (\text{J/m}\,\text{s}\,\text{K}) \tag{14}$$

The effective thermal conductivity of the fluid in the porous phase is calculated by [14]

$$\frac{k_2}{k_1} = \left(\frac{k_s}{k_1}\right)^{0.280 - 0.757\,\log\varepsilon - 0.057\log(k_s/k_1)} \tag{15}$$

where $k_s$ is the thermal conductivity of the porous material.

Table 2
Basic simulation conditions

| | |
|---|---|
| Inlet conditions | |
| Composition (vol.%) | 1.0% $CH_4$, 99% air |
| Temperature (K) | 700 |
| Pressure (atm) | 1.0 |
| Velocity (m/s) | 3.2 |
| Geometrical conditions | |
| Channel length, $L$ (m) | 0.04 |
| Channel radius, $R_2$ (mm) | 1.0 |
| Porous layer thickness, $(R_2 - R_1)$ (mm) | 0.30 |
| Catalyst support materials | |
| Tortuosity, $\tau$ | 4.0 |
| Porosity, $\varepsilon$ | 0.4 |
| Permeability, $K$ ($m^2$) | $1 \times 10^{-8}$ |
| Thermal conductivity, $k_s$ (W/(m K)) | 25 |

*Note:* the permeability value was taken in reference to wire crimps [14].

All the convective-diffusion type coupled differential equations were solved using the finite volume difference method and the SIMPLE algorithm. Details of the method may be found in [15]. The solution domain consisted of the porous layer and the bulk phase as a whole. An advantage of this treatment is that the uncertainties [16] encountered in determining the interface conditions between the fluid and the porous layer were avoided.

## 3. Results and discussion

### 3.1. Basic features of the velocity, temperature and concentration distributions

In this section, the velocity, temperature and concentration distributions from the present 2D simulations are presented. A summary of the basic simulation conditions is presented in Table 2.

Fig. 2 showed the typical axial velocity profile in the radial direction. It is noted that a retarded viscous flow exists in the porous layer, and thereby an increased bulk flow is found. Fig. 3 showed the variation in the temperature distribution. It is found that while the temperature gradient in the bulk phase is significant, but in the porous layer the temperature difference is very small. This is due to the high conductivity of the porous material selected, 25 W/(m K), which is a characteristic value for steel and alloys. Fig. 4 showed the variation in the concentration distribution. It is found that in the porous layer the concentration difference is very significant, while the concentration gradient in the bulk phase is small. It is notable that near the outer layer there exists a region where the reactant is nearly depleted.

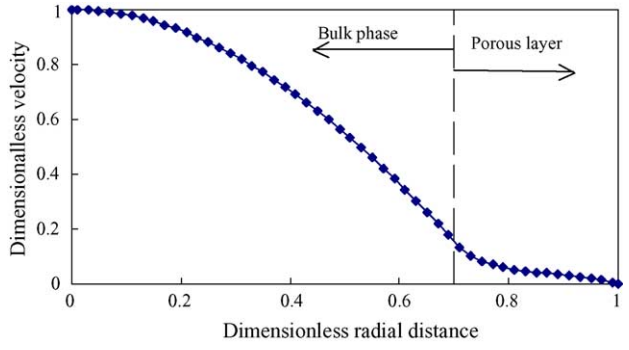


Fig. 2. Axial velocity distribution in the radial direction at a axial location $x = 0.0287$ m for the conditions listed in Table 2.

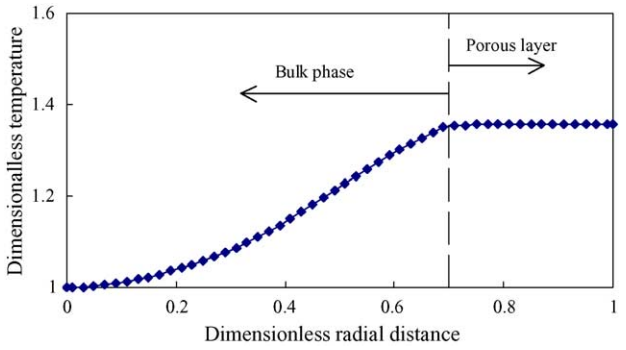


Fig. 3. Temperature distribution in the radial direction at a axial location $x = 0.0287$ m for the conditions listed in Table 2.

### 3.2. Fluid/porous surface mass transfer properties

In what follows, the derived parameters such as the Sherwood number and effective factor that characterize the reactor performances are discussed. First, the external mass transfer of the present two layer channel was compared with that of a monolith channel where only surface reaction occurs on the tube wall, i.e., the active layer is simplified to be a geometrical surface as studied by Hayes and Kolaczkowsik [8]. To evaluate the mass transfer between the bulk phase and the support surface, a Sherwood number is defined as

$$Sh_b = \frac{2R_1}{(\langle C_A \rangle_b - C_{Ai})} \left. \frac{\partial C_{A1}}{\partial r} \right|_{r=R_1} \tag{16}$$

where $C_{Ai}$ is the interface concentration between the bulk phase and the catalyst layer, and the bulk average

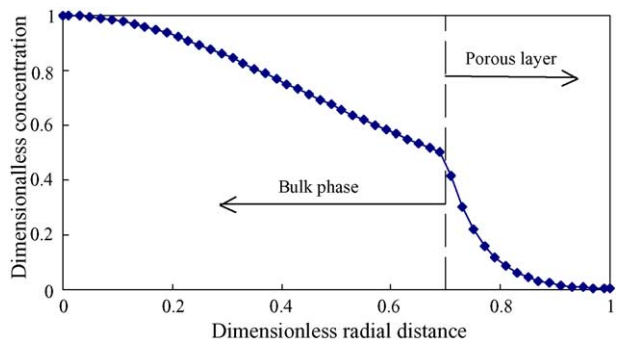


Fig. 4. Concentration distribution in the radial direction at a axial location $x = 0.0287$ m for the conditions listed in Table 2.

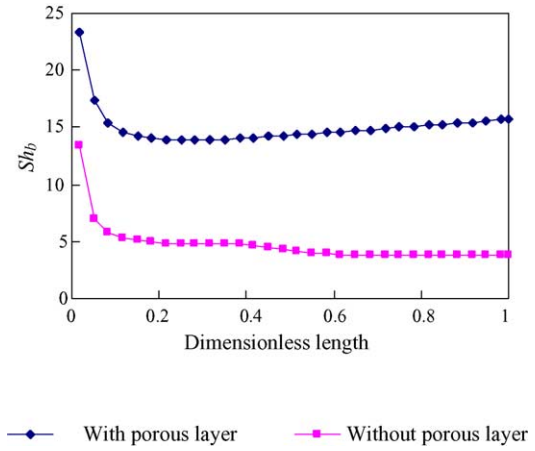


Fig. 5. Sherwood numbers between channel/catalyst layer interface along the channel axial length for the case shown in Table 2.

concentration $\langle C_A \rangle_b$ is

$$\langle C_A \rangle_b = \frac{\int_0^{R_1} u_1(r) C_{A1}(r) r \, dr}{\int_0^{R_1} u_1(r) r \, dr} \tag{17}$$

The $Sh_b$ values can be computed from the concentration field obtained by the solution of the governing equations. In Fig. 5, the Sherwood numbers were plotted as a function of the dimensionless axial distance along the channel length. From the figure it is seen that an increase in $Sh_b$ values by a factor of around 3 is obtained by the present design over the surface-reaction-only one. It is obvious that such an enhanced mass transfer between the bulk phase and the porous solid phase is due to a decrease in external film resistance. The following observations can be made about the results. In the latter case the Sherwood number predicted in the simulations is of the same order of magnitude as that predicted for the situation of constant wall temperature and constant wall flux.

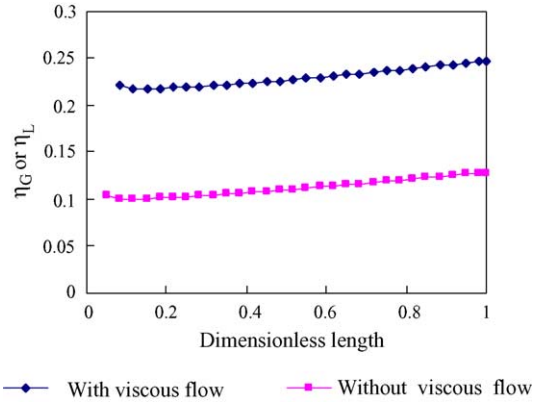


Fig. 6. Effective factors of catalyst layer along the channel axial length for the case shown in Table 2.

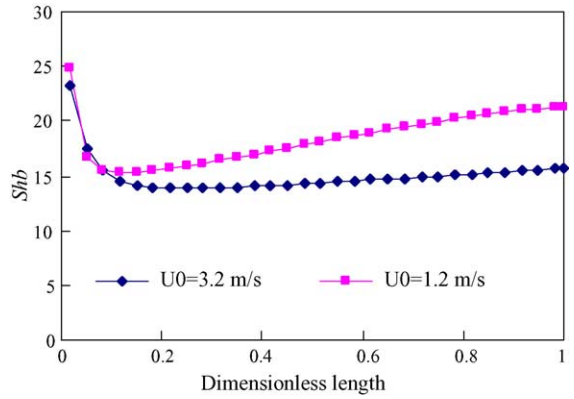


Fig. 7. Effect of inlet gas velocity on Sherwood number (otherwise noted in the figure, refer to Table 2 for complete simulation conditions).

### 3.3. Internal mass transfer properties within the porous support

The reaction performances of the present two layer channel was further compared with that of a monolith channel where there is a washcoat layer, that is coated onto the base substrate surface, but within the substrate no viscous flow (Darcy flow) is allowed. In the former case, to evaluate the internal mass transfer within the porous support, an effective factor is defined as

$$\eta_G = \frac{(2/(R_2^2 - R_1^2)) \int_0^{(R_2 - R_1)} r_A(x, r) r \, dr}{r_A(\langle C_A \rangle_b)} \tag{18}$$

where the bulk average concentration is the same as in Eq. (17). In the latter case, for a first order reaction in concentration, a generalized Thiele modulus can be defined as [9]

$$\phi_L = L_C \sqrt{\frac{k_V}{D_{AB,2}}} \tag{19}$$

where the character length, $L_C$, is the ratio of washcoat volume to fluid/porous surface area. The generic solution for

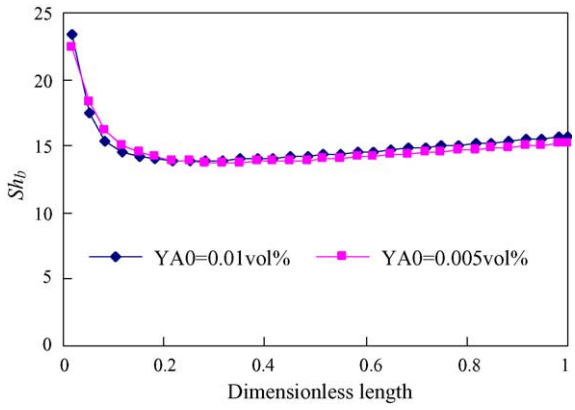


Fig. 8. Effect of inlet concentration on Sherwood number (otherwise noted in the figure, refer to Table 2 for complete simulation conditions).

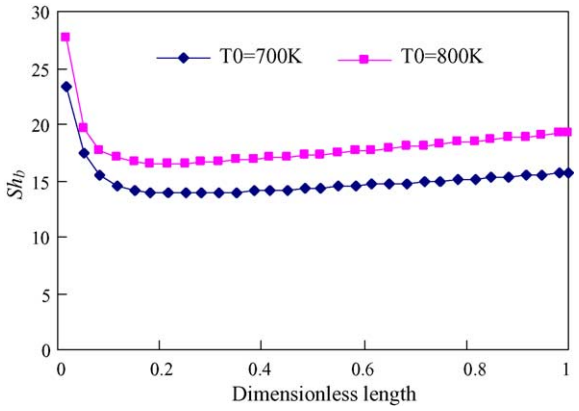


Fig. 9. Effect of inlet gas temperature on Sherwood number (otherwise noted in the figure, refer to Table 2 for complete simulation conditions).

the effective factor can be approximated in 1D using the analytical solution for an isothermal flat plate

$$\eta_L = \frac{\tanh(\phi_L)}{\phi_L} \tag{20}$$

Here, we used this expression to evaluate the effectiveness for the no viscous flow case. In Fig. 6, the Sherwood numbers were plotted as a function of the dimensionless axial distance along the channel length. From the figure it is seen that an increase in effective factor values by a factor of around two is obtained by the present design when the viscous flow within the porous layer is accounted for. Again, our simulations show that an enhanced mass transfer within the solid phase was obtained by the present design mainly due to the viscous flow effect within the porous solid.

Finally, the effects of inlet gas temperature, inlet concentration of methane and inlet velocity of the mixture on the external mass transfer of the present two layer channel were shown in Figs. 7–9. Varying the inlet velocity results in larger differences in $Sh_b$ in the developed flow region; see Fig. 7. The external mass transfer is not sensitive to the inlet concentrations; see Fig. 8. Higher inlet temperature yields high values of the predicted Sherwood number; see Fig. 9.

It is worth mentioning that the analysis presented above was developed for the case of a first order reaction. Changes in reaction type and flow duct shape may lead to more complicated situations.

## 4. Conclusions

Based on the work done and discussions presented, the following major conclusions can be drawn.

(1) It is obvious that an increased specific area available to reaction was obtained by the present configuration. More importantly, our simulations show that for the present design an enhanced mass transfer between the bulk phase and the porous solid phase due to a decrease in external film resistance between the bulk fluid and the catalyst layer.
(2) An enhanced mass transfer within the solid phase was obtained by the present design mainly due to the viscous flow effect within the porous solid.
(3) The effects of inlet gas temperature, inlet concentration of methane and inlet velocity of the mixture on the external mass transfer of the present two-layer channel is minor.

## Acknowledgement

This work is supported as a key project (No. 20136010) by the NSFC and also supported by the SINOPEC, China.

## References

[1] T. Boger, A.K. Heibel, C.M. Sorensen, Ind. Eng. Chem. Res. 43 (2004) 4602.
[2] F. Frauhammer, G. Eigenberger, L.V. Hippel, D. Arntz, Chem. Eng. Sci. 54 (1999) 3661.
[3] R.M. Heck, Chem. Eng. J. 82 (2001) 149.
[4] J.L. William, Catal. Today 69 (2001) 3.
[5] G. Groppi, E. Tronconi, Chem. Eng. Sci. 55 (2000) 2161.
[6] G. Groppi, A. Betolli, E. Tronconi, P. Forzatti, Chem. Eng. Sci. 50 (1995) 2705.
[7] R.E. Hayes, T.S. Kolaczkowski, Chem. Eng. Sci. 49 (1994) 3587.
[8] R.E. Hayes, S.T. Kolaczkowsik, Catal. Today (47) (1999) 295.
[9] R.E. Hayes, B. Liu, R. Moxom, M. Votsmeier, Chem. Eng. Sci. 59 (2004) 3169.
[10] L.L. Raja, R.J. Kee, O. Deutschmann, J. Wolf, L.D. Schmidt, Catal. Today (59) (2000) 47.
[11] M. Zanfir, A. Gavriilidis, Chem. Eng. Sci. 56 (2001) 2671.
[12] M. Zanfir, A. Gavriilidis, Chem. Eng. Sci. 58 (2003) 3943.
[13] M.K. Alkam, M.A. Al-Nimr, Int. J. Heat Mass Transfer 42 (1999) 3609.
[14] M. Kaviany, Principles of Heat Transfer in Porous Media, Springer-Verlag, Berlin, 1995 , p. 144.
[15] S. Patankar, Numerical Heat Transfer and Fluid Flow, Hemisphere Publishing Corporation, USA, 1980.
[16] C. Deng, D.M. Martinez, Chem. Eng. Sci. 60 (2005) 329.